



Polyethylene-BN nanosheets nanocomposites with enhanced thermal and mechanical properties



Md Golam Rasul ^a, Alper Kiziltas ^b, Christos D. Malliakas ^c, Ramin Rojaee ^a, Soroosh Sharifi-Asl ^a, Tara Foroozan ^a, Reza Shahbazian-Yassar ^{a,*}, Babak Arfaei ^{d, **}

^a Mechanical and Industrial Engineering Department, University of Illinois at Chicago, Chicago, IL, 60607, USA

^b Research and Innovation Center, Ford Motor Company, Dearborn, MI, 48124, USA

^c Department of Chemistry, Northwestern University, Evanston, IL, 60208, USA

^d Research and Advanced Engineering, Ford Motor Company, Palo Alto, CA, 94304, USA

ABSTRACT

Polyethylene (PE) are in demand for electrical insulation and thermal management applications; however, their low mechanical and thermal properties pose major challenges. Herein, we report on novel properties of PE-boron nitride (BN) nanocomposites prepared by melt compounding followed by injection molding. The thermal and mechanical properties of silane-functionalized (sBN) and non-functionalized (pBN) PE-BN nanocomposites were studied in order to assess the role of silane functional groups at the interface of BN nanosheets and PE matrix. In comparison with PE materials, addition of 5 wt % BN nanosheets increases tensile modulus of elasticity by 37 and 42%, flexural modulus of elasticity by 24 and 30%, tensile strength by 15 and 27%, and storage modulus by 80 and 91% for pBN and sBN nanocomposites, respectively. Besides mechanical reinforcement, thermal and thermomechanical properties were evaluated for PE-BN nanocomposites. While thermal stability of PE-pBN and PE-sBN nanocomposites was comparable, coefficient of thermal expansion was decreased by 12 and 20% at 5 wt % pBN and sBN nanosheets, respectively. These polymer nanocomposites with enhanced mechanical and thermal properties can be an excellent choice for application in insulation materials, including thermal interface layers in electronic devices.

1. Introduction

Recent advances in electronic devices have led to more demand in polymer materials like polyethylene (PE) for insulation and thermal management purposes [1–3]. Because of low permittivity and high electrical breakdown strength, PE is widely used as an insulation material [4,5]. However, low mechanical and thermal properties of PE polymer result in early mechanical failure during long term service [6, 7]. Boron nitride (BN) nanomaterials with outstanding mechanical properties (Young's modulus \sim 1 TPa), flexibility, high thermal stability (\sim 800 °C in air), low dielectric constant (\sim 4), high band gap (\sim 5.4 eV), high voltage breakdown strength (\sim 12 MV/cm), and chemical inertness are promising fillers to tune the mechanical and thermal properties of PE materials [8]. BN nanosheets have been used in polymer nanocomposite materials where thermal management, electrical resistivity, and dielectric properties are important.

In spite of the potential reinforcement effects of BN nanosheets in polymers, the incompatibility of inorganic BN nanosheets with organic polymer materials can cause the degradation in mechanical and thermal

properties of such nanocomposites [9,10]. For example, Wang et al. [11] reported degradation in mechanical properties of epoxy-BN nanosheets nanocomposites, where tensile strength and elastic modulus were reduced by 80 and 20% compared to the base epoxy polymer. Therefore, it is important to improve the compatibility by functionalizing BN nanosheets with appropriate coupling agents and enhance polymer-BN nanosheets interfacial interactions [12]. Organic polymer molecules such as PE and inorganic BN nanosheets have limited non-covalent interactions (e.g., van der Waals) due to their bond structure. As a result, chemically modifying BN nanosheets with appropriate functional groups are essential to enhance these non-covalent interactions [13]. Functionalization may also introduce new molecular interactions (e.g., hydrogen bonding, hydrophobic, and π - π interactions) and increase the degree of miscibility into polymer matrices that can contribute to the improvement of mechanical and thermal properties. Yu et al. [14] functionalized BN nanoplates with covalent, i.e., hyperbranched aromatic polyamide (HBP) and noncovalent, i.e., octadecylamine (ODA) ways to fabricate epoxy-BN nanoplates nanocomposites. This work reported 12.8 and 12.3% increase in storage modulus by the covalent and

* Corresponding author.

** Corresponding author.

E-mail addresses: rsyassar@uic.edu (R. Shahbazian-Yassar), barfaei@ford.com (B. Arfaei).

non-covalent functionalized BN nanoplates while the same property in the pristine BN nanoplates nanocomposites increased only by 7% at 5 wt % BN nanoplates, respectively. This improvement is believed to be originating from the enhanced interactions between epoxy and functionalized BN nanoplates. Depending on the compatibility of BN nanosheets with different polymer materials, nanocomposites were fabricated with wide range of BN functionalities, including $-\text{OH}$, $-\text{NH}_2$, $-\text{C}_4\text{H}_9$, $-\text{F}$, $-\text{CH}_3(\text{CH}_2)_{17}\text{NH}_2$, $-\text{C}_9\text{H}_{23}\text{N}_2\text{O}_3\text{Si}$ [15–17]. Huang and co-workers [18] reduced the interfacial thermal resistance of epoxy-BN nanocomposites by modifying BN with polyhedral oligosilsesquioxane molecules. The 29% decrease in coefficient of thermal expansion (CTE) and 1360% increase in thermal conductivity were achieved at 30 wt % BN mass loading by the effective BN surface modification.

Silane functionalization is an attractive choice for modifying BN nanosheets due to the functional groups that can bond and interact with both organic and inorganic compounds [19]. Silane functionals have organic alkyl molecules ($-\text{R}$), which are very compatible with polyethylene molecules due to nonpolar chemical structure. Additionally, silane contains oxygen molecules which are electronegative and may create Hydrogen-bond between polymer materials and BN nanosheets; these increase molecular interactions and enhance nanocomposite performances [20–22]. In spite of few reports on the reduction of interfacial thermal resistance for PE-BN nanocomposites [20,23], these studies lack detailed analyses of thermal stability, thermomechanical and mechanical performances. The objective of this work is to investigate the effects of silane functionalization (3-aminopropyltriethoxy silane) on mechanical and thermal properties for PE-BN nanocomposites. The PE-BN nanocomposites were fabricated via melt compounding method utilizing industrially available PE polymer materials. Their mechanical and thermal properties were thoroughly evaluated in terms of tensile modulus of elasticity (TMOE), flexural modulus of elasticity (FMOE), tensile strength, storage modulus, coefficient of thermal expansion (CTE), and thermal stability using tensile and flexural, DMA, DSC, and TGA tests.

2. Experimental

2.1. Materials

PE polymers were kindly received from an industrial supplier, which were used to fabricate PE nanocomposites. This PE is usually used for cable insulation material for automotive applications. The detailed characterization of the as-received PE samples is shown in **Supplementary Information** (Fig. S1, S2, and S3). The scanning electron microscopy (SEM) image (Fig. S1) and thermogravimetric analysis (TGA) (Fig. S2) indicate that the as-received PE material contains ~ 37 wt % inorganic residues. The SEM-EDS mapping (Fig. S3) suggests that most of these residues are likely to be aluminium oxide (Al_2O_3) and zinc oxide (ZnO). In this study, the pristine BN (pBN) and silane-modified BN (sBN) nanosheets were used to fabricate polymer nanocomposites. These BN nanosheets were purchased from US Research Nanomaterials Inc. and added to the PE during nanocomposite compounding. Both pristine and silane-modified BN nanosheets are hexagonal crystal structure, and the average lateral sizes are 100–200 nm. Silane modified BN nanosheets were modified by functionalizing with 1–3 wt % silane coupling agent (KH-550) using 3-aminopropyltriethoxysilane ($\text{C}_9\text{H}_{23}\text{N}_2\text{O}_3\text{Si}$, CAS: 919-30-2). Both pristine and silane-modified BN nanosheets were 99.8% pure. The polymer and BN nanosheets were dried in air at 80°C for 6–8 h before melt compounding.

2.2. Fabrication of polymer nanocomposites

An appropriate amount of dried PE pellets and BN nanosheets were fed into the K-Tron (Coperion, Stuttgart, Germany) gravimetric feeders separately to compound the master batch of 5 wt % PE-BN nanocomposites. In order to fabricate a homogenous mixture of

nanocomposites, the speed of the gravimetric feeder was optimized. Twin-screw extruder (ThermoHaake Rheomex Model PTW25, St. Louis, MO, USA) was used to compound the master batch of 5 wt % PE-BN nanocomposites. Extruded melt compounded product streams were cooled down through a room temperature water bath and granulated using a Nelmor lab-scale grinder (AEC, New Berlin, WI, USA). The grinded master batch nanocomposites were dried in an oven at 60°C for at least 12 h before further processing. The rest of the nanocomposites were prepared by mixing appropriate amount of master batch nanocomposites (5 wt % PE-BN) and PE polymer utilizing twin-screw extruder. Extrusion was carried out with a barrel temperature range of 185–200 °C at 120 rpm screw speed. The maximum pressure in barrel was set to 70 MPa for compounding nanocomposites. Later, an injection molding machine (Boy Machines, Model 80 M, Exton, PA, USA) was used to prepare specimens for mechanical and thermal characterizations. The barrel temperature for injection molding was in the range of 205–215 °C. The cooling time was 30 s, with a mold temperature of 50 °C. Base PE materials (without BN nanosheets) were prepared following the same procedures to have the similar thermal and processing history. The PE nanocomposites are labeled in the format of PE-weight percentage of BN nanosheets, type of BN nanosheets (pBN or sBN). For example, PE-5.0 wt % pBN indicates that this nanocomposite is composed of polyethylene polymer and 5 wt % pristine BN nanosheets. Simply PE-BN indicates that the PE-BN nanocomposite is prepared with PE and BN nanosheets (i.e., either pBN or sBN nanosheets).

3. Results and discussion

3.1. BN nanosheets characterization

Fig. 1a–c shows the morphology and structure of BN nanosheets before addition into PE polymer matrix. The average lateral sizes of the BN nanosheets are in the range of 100–200 nm. Atomic resolution low-angle annular dark field (LAADF) image (Fig. 1b) depicts the crystalline nature of BN nanosheet with a six-fold symmetry in the indexed fast Fourier transform (FFT) image (inset in Fig. 1b), confirming the hexagonal crystalline structure of BN nanosheets with a lattice spacing of 0.246 nm. Height profile was also obtained from atomic force microscope (AFM) data, and the average thickness of BN nanosheets is 50 nm (Fig. 1c). These morphological characteristics (i.e., higher surface area) are essential for interacting with polymer chains and, thus, desirable for polymer nanocomposite applications.

Chemical bonding and molecular interactions for pBN and sBN nanosheets were compared to better understand the silane functionalization. The high-intensity Fourier transform infrared (FTIR) spectra at 1384 and 808 cm^{-1} (Fig. 1d) for both pBN and sBN nanosheets are attributed to in-plane B–N stretching and out of plane B–N–B bending vibration [21]. The peak at 3427 cm^{-1} indicates the $-\text{OH}$ group, and the peak at 1616 cm^{-1} (inset in Fig. 1d) is attributed to $\text{N}-\text{H}^+$ vibration mode [21]. The Si–O stretching bond information is shown at 1100 cm^{-1} for sBN nanosheets. This weak intensity of the peak at 1100 cm^{-1} is possibly due to the intensive characteristics of BN nanosheets. A slight shift of IR spectra (1384 – 1396 cm^{-1}) at in-plane B–N stretching is assumed to be originating from the new covalent bond formation due to silane grafting on BN nanosheets [21]. Further, time-of-flight secondary ion mass spectra (ToF-SIMS) analysis was conducted to confirm the presence of elemental molecules on BN nanosheets. Both the positive and negative ion spectra were collected to identify the chemical states of the functionalization. Fig. 1e exhibits the presence of Si molecules on sBN nanosheets. X-ray photoelectron spectroscopy (XPS) analysis was performed to further confirm the silane functionalization. Silane molecules react with BN nanosheets and form covalent bonds with boron molecules. The binding energy is measured by XPS and demonstrated in Fig. 1f–h. Fig. 1f indicates B 1s spectrum of pBN nanosheets while B 1s spectrum of sBN nanosheets can be fitted into B–N and B–O bonding (Fig. 1g). Because of the covalent bond of silane molecules with B atoms,

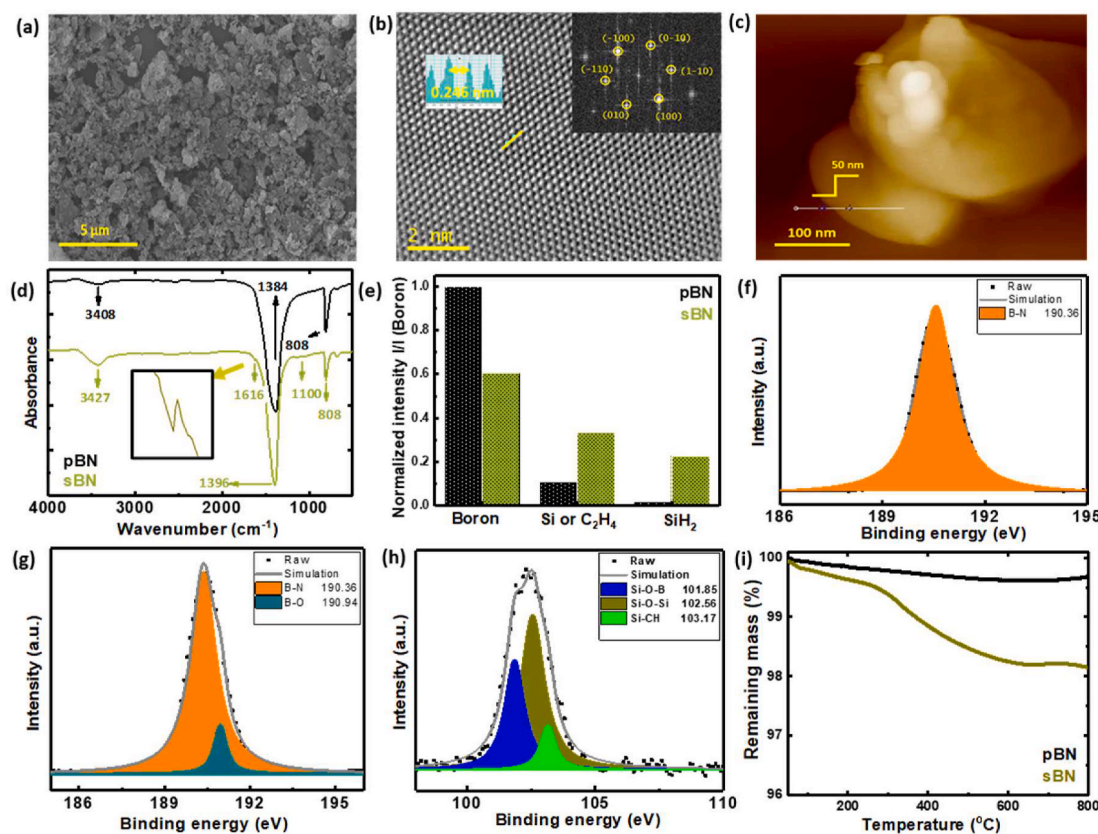


Fig. 1. Characterization of pristine and silane functionalized BN (pBN and sBN) nanosheets: (a) SEM micrograph of BN nanosheets showing shapes and sizes; (b) atomic resolution LAADF image of BN nanosheet (inset shows d -spacing of BN nanosheet atoms and crystal structure with a zone axis of [001] for hexagonal BN nanosheet in FFT); (c) AFM micrograph of BN nanosheets with corresponding thickness 50 nm; (d) FTIR spectra of pristine and surface functionalized BN nanosheets, strong BN peaks at 1384 and 808 cm^{-1} region overlaps with weak silane peak (Si-O stretching) at 1100 cm^{-1} and $\text{N}-\text{H}^+$ peak at 1616 cm^{-1} ; (e) relative intensities of boron, Si/C₂H₄, and SiH₂ spectra based on positive ToF-SIMS fragments for pBN and sBN nanosheets. Intensities are normalized to boron peak of pBN nanosheets; (f) XPS B 1s spectrum for pBN nanosheets indicates only B-N bonding; (g) XPS B 1s spectrum for sBN nanosheets, the deconvoluted curve indicates B-N and B-O bonding; (h) XPS Si 2p spectrum for sBN nanosheets, the deconvoluted curve indicates Si-O-Si, Si-O-B, Si-CH₂ bonding; (i) TGA thermogram for surface-functionalized and pristine BN nanosheets depicts the functionalization is ~ 1.7 wt %.

these two B-N and B-O bonds are appeared on sBN nanosheets. To further illustrate the silane bonding with BN nanosheets, Fig. 1h demonstrates Si 2p spectrum for sBN nanosheets. The deconvoluted peaks (Si-O-Si, Si-O-B, and Si-CH₂ bonding) reiterate the successful grafting of silane molecules on BN nanosheets. In addition, survey spectra of both pBN and sBN nanosheets show the presence of B, N, C, and O (Fig. S4) molecules. Owing to the chemical structure of silane functionalized BN nanosheets, the peak intensities of C 1s and O 1s are higher for sBN compared to pBN nanosheets. These observations confirm that the silane was successfully grafted onto the BN nanosheets. Besides, the morphology and lattice structure of BN nanosheets have been tested before and after functionalization using SEM, TEM, and X-ray diffraction (XRD). The SEM images of pBN and sBN nanosheets confirm that the functionalization does not affect the size of BN nanosheets (Fig. S5). In addition, AC-STEM images (Fig. S6) and XRD peak analysis (Fig. S7 in Supporting Information provides details of XRD peak analysis) confirm that the silane functionalization does not change the lattice integrity of BN nanosheets. Also, there is no change in d -spacing of BN nanosheets after functionalization, indicating that the silane functional molecules are attached on the surface of BN nanosheets.

Quantitative analysis of silane functionalization was performed to assess the amount of silane grafting on BN nanosheets. TGA graph (Fig. 1i) indicates thermal stability of both pBN and sBN nanosheets. Because of the presence of hydroxyl molecules, surface-functionalized BN nanosheets exhibit a weight loss starting at 100 °C. Fig. 1i indicates that sBN nanosheets start to lose mass at ~ 250 °C and continue

up to 600 °C, at which point approximately 2 wt% of the initial mass is lost. Whereas pBN nanosheets exhibit nearly no change in the weight loss up to 800 °C where 99.68% of initial weight is retained. This indicates that the silane functionalization is estimated to be ~ 1.7 wt %, which is very low and complies with weak spectra reported in both FTIR and ToF-SIMS analysis. The electronic structure of BN nanosheets is the possible reason behind this low grafting of silane. Since weak organic-inorganic interaction of polymer-BN nanosheets plays an unfavorable role in boosting mechanical and thermal properties of bulk nanocomposites [24]. In this work, this challenge was overcome by utilizing silane functionalized BN nanosheets. A schematic illustration of BN nanosheets modification is shown in Fig. 2a. Functionalization of BN nanosheets (Fig. 2a) indicates the presence of organic molecules on inorganic BN nanosheets, which increase the miscibility and enhance interactions with various organic solvents. As seen in Fig. S8, the surface-functionalized sBN nanosheets disperse into organic solvents such as tetrahydrofuran (THF) uniformly compared to pBN nanosheets due to polar-polar interactions, indicating increased dispersibility of sBN nanosheets [18].

3.2. Mechanical characterization

The non-linear mechanical reinforcement of pBN and sBN nanosheets was analyzed to show the effect of silane functionalization on PE matrix chain mobility. Because of the molecular chain structure, the base PE matrix has very low TMOE (~ 316 MPa), FMOE (~ 292 MPa),

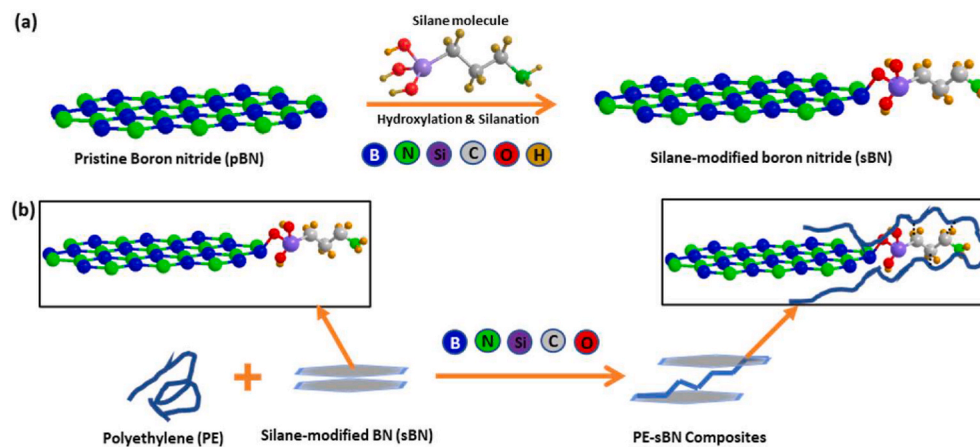


Fig. 2. Schematic illustration of surface functionalization of BN nanosheets and polymer-BN nanosheets interactions: (a) schematic of silane functionalization of BN nanosheets; (b) PE-sBN nanocomposites fabrication and interfacial molecular interaction. The molecular interactions between silane molecules of BN nanosheets and PE chains at PE-sBN interfaces are higher when compared with PE-pBN interfaces. The left inset (Fig. 2b) shows the chemical structure of silane-modified BN nanosheets, and the right inset shows PE chain interaction with silane functionalized BN nanosheets.

and tensile strength (~ 11 MPa). This means that the molecular chains within the polymer face little difficulty to move or relax under an applied load [25]. The stress-strain curves for PE-BN nanocomposites are shown in Fig. 3a. Fig. 3a indicates that the mechanical properties of PE-BN nanocomposites are increased with an expense of ductility. While FMOE was calculated from a 3-point bending test and plotted in Fig. 3b, TMOE and tensile strengths are calculated from stress-strain curves (Fig. 3a) and plotted in Fig. 3c-d. Once pBN nanosheets are added into the base PE matrix, it is demonstrated that the FMOE (Fig. 3b) and TMOE (Fig. 3c) are reported an increment of 37% and 24% compared to the base PE matrix, respectively. Similarly, tensile strength is also increased by 15% (Fig. 3d), and all of these improvements are realized at 5 wt % pBN nanosheets. Differential scanning calorimetry (DSC) and XRD analysis of PE and PE-BN nanocomposites were conducted to evaluate the effect of the percentage of crystal regions and crystallite sizes (details of calculations and results are provided in Supplementary Information). As shown in Table S1, there is little change in the percentage of crystal regions and crystallite sizes between PE and PE-BN nanocomposites. Therefore, the reinforcement of BN nanosheets is not

likely originating from either the percentage of crystal region or crystallite size, as reported in [26]. This means that the entanglement of pBN nanosheets into PE chains creates obstacles for the movement of the chains under applied tensile load. Polymer chain entanglement originating from weak interactions between pBN nanosheets and PE matrix explains this increase in mechanical properties of nanocomposites [27]. Interestingly, the silane-modified BN nanosheets enhance these mechanical properties of nanocomposites even further compared to pBN nanosheets (Fig. 3a-d). For example, FMOE and TMOE of PE-5.0 wt % sBN nanocomposites are increased by 30 and 42% and tensile strength is increased by 27% compared to the base PE matrix, respectively. Thus, sBN nanocomposites show 5.5% increase in FMOE, 3.7% increase in TMOE, and 11% increase in tensile strength in comparison to pBN nanocomposites at 5.0 wt % BN nanosheets.

The fractography of the PE, PE-5.0 wt % pBN, and PE-5.0 wt % sBN nanocomposites were investigated to uncover the polymer chain deformation during tensile fracture using SEM micrographs (Fig. 4a-h). The surface morphology of the fractured PE-BN (PE-5.0 wt % pBN and PE-5.0 wt % sBN) nanocomposites indicates a limited plastic

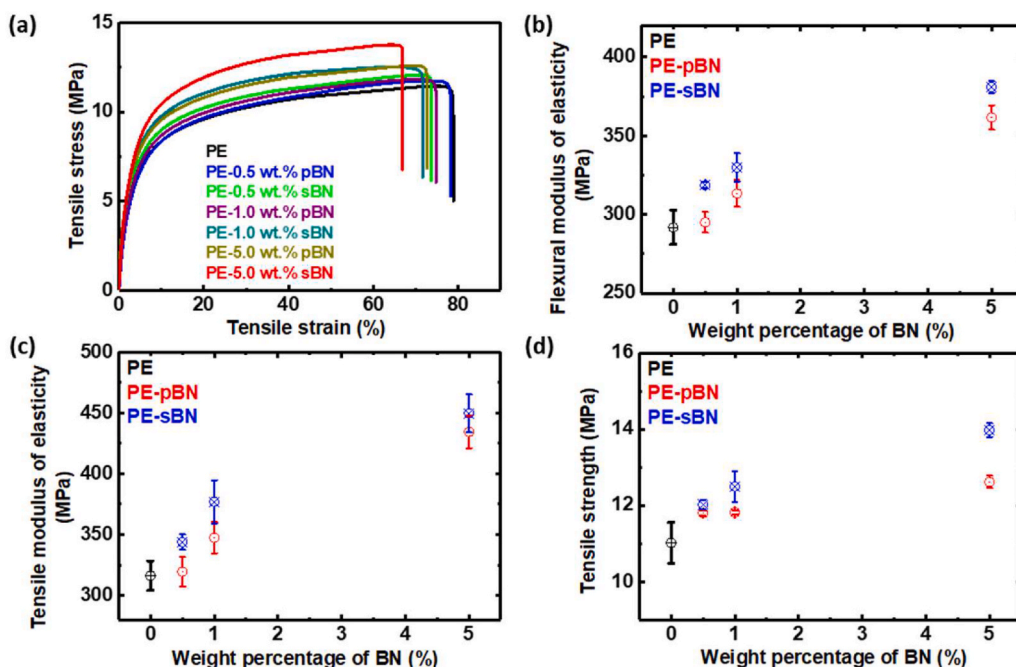


Fig. 3. Mechanical characterization of the PE and PE-BN nanocomposites: (a) stress-strain curves for the PE matrix and the PE nanocomposites at 0.5, 1, and 5 wt % BN nanosheets loading; (b) FMOE, (c) TMOE, and (d) tensile strength with varying compositions of both sBN and pBN nanosheets.

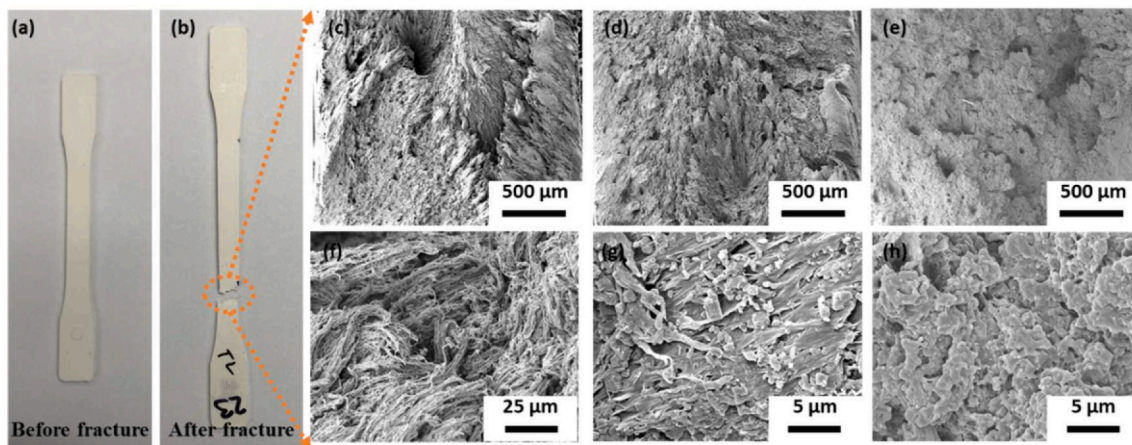


Fig. 4. Morphological characterization of the fractured PE and PE-BN nanocomposites. Optical images of PE-BN nanocomposites: (a) before tensile fracture, (b) after tensile fracture. SEM micrographs of tensile fractured surfaces of (c) PE, (d) PE-5.0 wt% pBN, and (e) PE-5.0 wt% sBN nanocomposite. Magnified SEM micrographs of Figure a, b, and c are shown in Figure (f), (g), and (h), respectively.

deformation, which implies a brittle behavior of fracture. In sharp contrast, the base PE specimen shows a fibrous morphology, indicating an extensive deformation before the fracture. In addition, a close examination of the fractured surfaces reveals that the plastic flow characteristics are more noticeable for PE-5.0 wt % pBN when compared to PE-5.0 wt % sBN nanocomposites. The mechanical interlocking characteristic of pBN nanosheets reduces the matrix mobility within nanocomposites, thus reducing its ductility when compared to PE. However, if the adhesion between fillers and matrix is not sufficient, extensive delamination will usually occur between the polymer matrix and fillers [28]. Whereas PE-sBN nanocomposites show the least plastic deformation among all nanocomposites (PE, PE-pBN, and PE-sBN

nanocomposites), indicating an enhanced interfacial adhesion between PE matrix and sBN nanosheets. Moreover, the XRD peak analysis of the PE and PE-BN nanocomposites were conducted to observe the PE polymer chain organization because of BN nanosheets addition (details of the XRD analysis and results are shown in **Supplementary Information**). As shown in **Fig. S10**, the addition of pBN and sBN nanosheets into PE materials results in no new peak because of three possible reasons: (i) overlapping with the peaks of ZnO and Al₂O₃, (ii) exfoliated dispersion state of BN nanosheets, and (iii) low content of BN nanosheets [29]. The reduction of the peak intensity at the 20 value of 26.81° could be attributed to the possible exfoliation of the sBN nanosheets compared to pBN into PE materials [30]. In addition, the peak intensity reduction

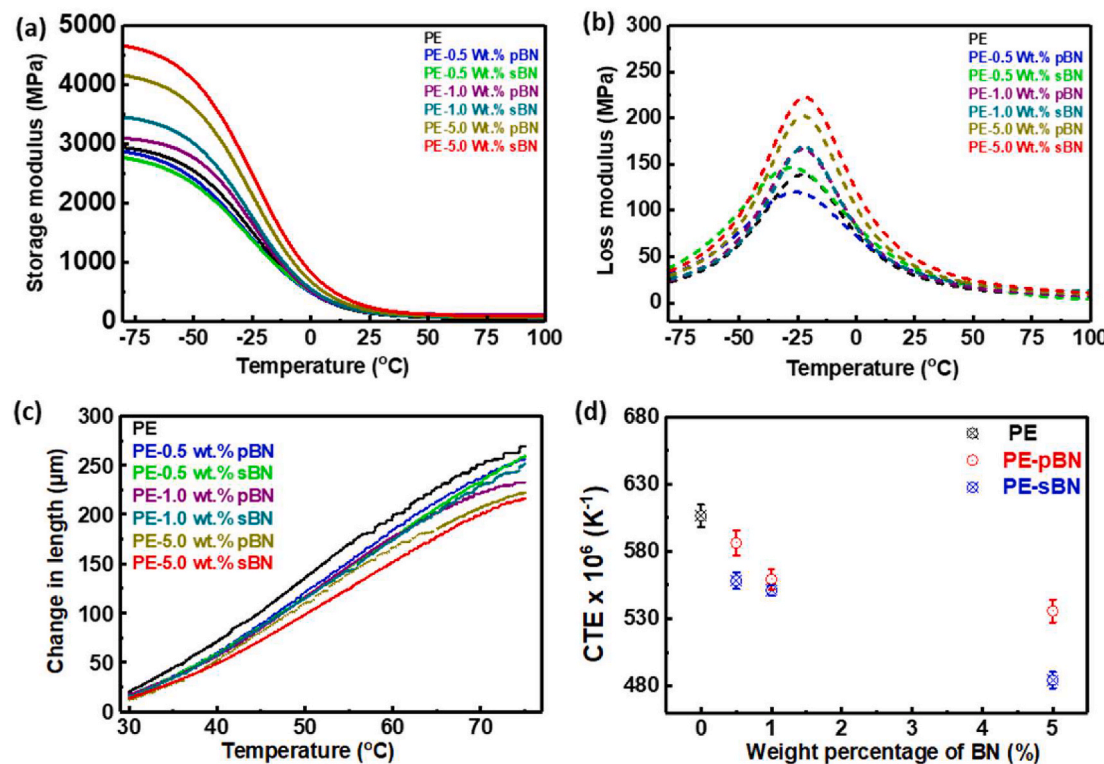


Fig. 5. Thermomechanical characterization of the PE and PE-BN nanocomposites: (a) storage and (b) loss modulus of PE-BN nanocomposites with increasing temperature from -80 to 100 °C; (c) changes in lengths with increasing temperature from 30 to 75 °C; (d) calculated CTE based on linear region (35–65 °C) of data in (c) is plotted against weight percentage of BN nanosheets.

of PE crystalline structure (2θ value of 21.3° and 23.4°) could be the result of the better compatibility of silane-modified BN nanosheets with PE matrix [31]. Such compatibility is likely resulting from the molecular interactions between PE matrix and sBN nanosheets, as also reported for other nanocomposite systems [31,32]. As a result, a higher TMOE, tensile strength, and FMOE are obtained for the PE-sBN when compared to the PE-pBN nanocomposites, which is in agreement with reported observations for other polymer nanocomposite systems [33].

To reveal the load transfer efficiency and polymer chain interactions with BN nanosheets, thermomechanical properties (i.e., storage modulus and loss modulus) were investigated [34]. Since storage and loss modulus require measuring stored elastic and dissipated energy during straining, molecular orientation and relaxation processes information can reveal chain mobility during transition periods. The changes in storage modulus (Fig. 5a) and loss modulus (Fig. 5b) for silane-modified BN nanosheets compared to pristine BN nanosheets nanocomposites are significant. In the rubbery state at 25°C , the storage modulus of sBN nanocomposites is increased by 36% (218–296 MPa) at 1 wt % BN nanosheets loading level compared to pBN nanosheets. More significant changes are observed at below -40°C , where friction between polymer chains is more prominent, and higher storage modulus is observed. Besides entanglements, the higher noncovalent interaction may increase the storage modulus in sBN compared to pBN nanocomposites due to efficient stress transfer from sBN nanosheets to polymer matrix [14]. Hence, the storage modulus of PE-sBN is higher compared to PE-pBN nanocomposites. Besides, loss tangent ($\tan\delta$) was calculated from the ratio of loss modulus to storage modulus and reported in Fig. S11. The $\tan\delta$ could provide glass transition temperature (T_g) of a material where T_g is determined from the peak temperature of the curves, as reported in many reports [21]. Although Fig. S11 shows $\tan\delta$ of PE and PE-BN composites with the increasing temperature from -80 to 100°C ; however, this graph does not show any peak in the glassy-rubber region of the samples. It is likely that the test temperature of the $\tan\delta$ curve (-80 to 100°C) was not sufficient to elucidate the glass transition temperature of the PE and PE-BN nanocomposites, since T_g of the polyethylene matrix usually occurs at around -115°C [35]. The slightly decreased $\tan\delta$ value of sBN nanocomposites compared to pBN indicates increased molecular interactions between PE and sBN nanosheets [21]. The silane molecule contains organic and inorganic functional groups, which act as a coupling agent and are likely to increase molecular interactions between organic PE polymer matrix and inorganic BN nanosheets [24]. The gap between PE and BN nanosheets is reduced due to these increased molecular interactions and leads to create an immobile phase (interphase) at the PE-sBN interface [36]. Thus, an efficient stress transfer could be originated at the interphase, and nanocomposites show reinforced mechanical properties with reduced chain mobility within nanocomposites. The reduced chain mobility will also lead to decrease CTEs [37]. Since BN nanosheets have very high specific surface area ($\sim 2600\text{ m}^2/\text{g}$) and silane functionalization leads to the formation of an immobilized phase at the interface in comparison to PE-pBN case [38]. The higher molecular interactions at the PE and sBN nanosheets interface can effectively restrain polymer chain dynamics.

3.3. Thermal characterization

The coefficient of thermal expansion was investigated to further understand the effects of BN nanosheets and their functionalization on thermomechanical stability of nanocomposites. CTE is an important parameter of polymer material that gives not only fundamental information about chain dynamics, but also important dimensional stability associated with heat. As shown in Fig. 5c, the changes in length for PE and nanocomposites are reported over the temperature range from 30 to 75°C . The linear region of Fig. 5c (35 – 65°C) was fitted, and CTEs were calculated from their slopes. As it can be observed (Fig. 5d), the CTE of base PE is $607 \times 10^{-6}\text{ K}^{-1}$. By adding BN nanosheets, CTE decreases

monotonically down to $484 \times 10^{-6}\text{ K}^{-1}$. Similar to what was observed in mechanical properties, sBN outperformed pBN nanocomposites in decreasing CTEs of PE nanocomposites at each of the concentrations of BN nanosheets (Fig. 5d). With 5.00 wt % BN nanosheets, pBN nanocomposites demonstrate CTE as $536 \times 10^{-6}\text{ K}^{-1}$ while sBN nanocomposites exhibit $484 \times 10^{-6}\text{ K}^{-1}$. This is 12 and 20% decrease in CTE of pBN and sBN nanocomposites in comparison to base PE. The physical entanglement of polymer chains induced by BN nanosheets and increased molecular interactions of silane functional groups with the PE matrix (Fig. 2b) could explain this significant reduction in CTE compared to the pBN nanocomposites [39].

Thermal degradation was explored to further understand the thermal stability of polymer materials and the role of silane grafting. Analyzing the thermal decomposition of pBN and sBN nanocomposites (Fig. 6a), it is evident that the degradation is a two-stage process, and the mechanism is not affected due to BN nanosheets addition. The addition of BN nanosheets increases the thermal stability of PE nanocomposites structures irrespective of functionalization. For example, the first onset temperature (T_{onset}) is shown in Fig. 6c, where T_{onset} indicates the starting of the 1st stage degradation of the materials. The result indicates that the decomposition process is delayed by adding BN nanosheets. T_{onset} of base PE matrix exhibits 268°C . By the addition of 1 wt % pBN nanosheets, T_{onset} is increased by 12°C . Further addition of pBN nanosheets (e.g., 5 wt %) does not enhance the thermal stability beyond PE-1.0 wt % pBN nanocomposites. This observation can be explained knowing that BN nanosheets can act as gas barriers and play a crucial role in increasing the thermal stability of nanocomposites [40]. A well tortuous path created by BN nanosheets into PE matrix enhances thermal stability by delaying the escape of decomposed volatile gases [41]. At the beginning of the degradation process (i.e., onset degradation), barrier nature of BN nanosheets obstructs volatile gas flow within the polymer matrix and results in delayed decomposition.

Likewise, the second onset temperature ($T_{20\%}$) (i.e., 20% weight loss temperature) where the materials start to degrade of its 2nd stage is also analyzed (Fig. 6d). Interestingly, higher improvement (thermal degradation temperature) is achieved for thermal stability at 20% weight loss compared to T_{onset} . For instance, the addition of 1 wt % pBN nanosheets increase T_{onset} of nanocomposites by 12°C while $T_{20\%}$ is improved by 18°C . This may be explained by the formation of chars (Fig. 6a), which likely act as volatile gas barriers [40,42]. Thus, BN nanosheets, along with chars, delay the escaping of volatile gases and reduce the decomposition of PE matrix at $T_{20\%}$. Interestingly, the PE-sBN nanocomposites do not show improvement in thermal weight loss over PE-pBN nanocomposites. Both T_{onset} and $T_{20\%}$ show almost similar behavior and increment of 16 and 18°C for $T_{20\%}$ for both sBN and pBN nanocomposites. This slight early degradation of sBN compared to pBN nanocomposites can be explained by the thermal degradation behavior of silane molecules. The thermal stability of sBN nanosheets (Fig. 1i) indicates that the degradation of silane starts at $\sim 250^\circ\text{C}$ [43]. This early degradation of silane alters the polymer-BN nanosheets interface and triggers the degradation of sBN nanocomposites at a slightly lower temperature compared to pBN nanocomposites. Similar results were also reported by Xie et al. [44,45] for thermal decomposition of long carbon-chain alkyl quaternary ammonium ions modified montmorillonite (MMT). The authors found that the weakly bonded water molecules were decomposed in the temperature region below 200°C , which is the possible reason for the early degradation of the polymer nanocomposite materials. Although the thermal stability of sBN nanocomposites is comparable to pBN nanocomposites. Yet, both pBN and sBN nanosheets show a moderate improvement in thermal stability performance. Besides the fact that the mass barrier property of BN nanosheets plays a crucial role in reducing thermal degradation, high thermal stability, and nanostructured morphology of BN nanosheets are also believed to be the other important reasons for enhanced thermal stability.

Overall, the addition of BN nanosheets into PE polymers enables

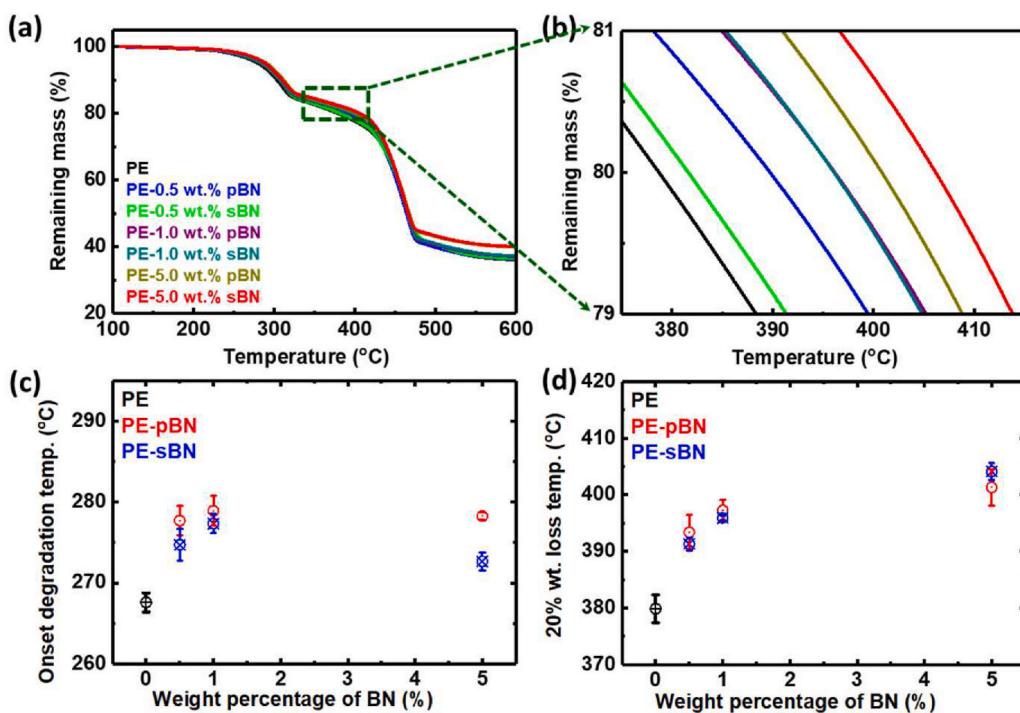


Fig. 6. Thermal stability analysis of PE and nanocomposites: (a) thermogravimetric analysis of the PE matrix and the PE nanocomposites; (b) enlarged area at 20% weight loss region; (c) 1st onset degradation temperature (T_{onset}); and (d) 2nd onset degradation ($T_{20\%}$) (i.e., 20% weight loss) temperatures are reported with varying concentrations of both sBN and pBN nanosheets.

nanocomposites with enhanced mechanical, thermomechanical, and thermal properties. However, the extent of improvement closely depends on PE-BN nanosheets interfacial molecular interaction. In this work, silane functionalized BN nanosheets were used to enhance this interaction. We obtained higher mechanical properties (TMOE, FMOE, and tensile strengths), thermomechanical properties (storage modulus), and lower CTE compared to PE-pBN nanocomposites. Unlike other 2D materials, BN nanosheets and their polymer nanocomposites are electrically insulative [1,46–48]. These mechanically strong, thermally, and dimensionally stable nanocomposite materials are promising in applications ranging from insulation materials (e.g., cable insulation), thermal management (e.g., heat transfer equipment) to electronic devices (e.g., thermal interface materials) [49–51]. While this study provides adequate insight on the role of silane functionalization groups, it would be interesting to study the effects of BN nanosheets over a broader range of BN nanosheets mass fraction to fully elucidate the silane functionalization effect on the properties of PE-BN nanocomposites.

4. Conclusions

In this work, the mechanical, thermomechanical, and thermal properties of PE polymer nanocomposites reinforced with silane functionalized and pristine boron nitrides were studied. Substantial improvements in the mechanical properties of PE-BN nanocomposites were achieved. In nanocomposites with 5 wt % pBN and sBN nanosheets, TMOE increased by 37, 42%, FMOE improved by 24, 30%, and tensile strength increased by 15, 27%, respectively. While thermal stability improvements are nominal (e.g., $T_{20\%}$ increased by 18, 16 °C for 1 wt % pBN and sBN nanosheets, respectively), the reductions in nanocomposites' CTE are compelling (e.g., pBN and sBN nanosheets reduce CTE by 12% and 20%, respectively). The chain mobility is also reduced because of the BN nanosheets addition, as evidenced from the increased storage modulus of pBN and sBN nanocomposites compared to PE. These enhancements in mechanical and thermal properties are likely originated not only from the outstanding mechanical, physical, thermal, and chemical properties of BN nanosheets, but also from the molecular

interaction of silane modified BN nanosheets with base PE matrix.

Declaration of competing interest

The authors declare that they have no known competing financial interests or personal relationships that could have appeared to influence the work reported in this paper.

Acknowledgements

This project is financially supported by Ford Motor Company. The efforts of R. Rojaee, S. Sharifi-Asl, and T. Foroozan were supported partially through NSF DMR-1809439 and NSF CBET-1805938. The fabrication of polymer nanocomposites and part of mechanical characterizations were carried out at Ford Research and Innovation Center, Dearborn, MI. Parts of the characterization works were carried out at the Soft Matter Characterization Facility of the University of Chicago, and Northwestern University Atomic and Nanoscale Characterization Experimental Center (NUANCE) of the Northwestern University. This work also made use of the JEOL JEM-ARM200CF in the Electron Microscopy Core of UIC's Research Resources Center and IMSERC facility at Northwestern University. Babak Arfaei would like to thank the Polymers and ESE teams at Ford, specially Matthew Volpone, for providing valuable feedback. The authors acknowledge Aptiv Co. in Warren, OH for providing samples. The authors also acknowledged insightful discussion with Dr. Philip J. Griffin at SMCF lab of the University of Chicago, Dr. Tamrakar Sandeep, and their team at the Research and Innovation Center of Ford Motor Company, and Dr. Xinqi Chen at Northwestern University for their valuable discussions.

Appendix A. Supplementary data

Supplementary data to this article can be found online at <https://doi.org/10.1016/j.compscitech.2020.108631>.

Authors statement

M.G.R., A. K., B.A., and R.S.Y. initiated the idea and designed the experimental protocols. M.G.R. and A.K. compounded the nanocomposites, carried out tensile, flexural tests. M.G.R. performed and analyzed SEM, ToF-SIMS, XPS, TGA, DMA. C. D. M. performed the XRD and M.G.R. did the result analysis. M.G.R and R.R. performed FTIR analysis. M.G.R and S.S carried out STEM and result analysis. M.G.R. and T.F. performed A.F.M. All the authors contributed to the revision and discussion of the manuscript.

References

[1] C. Zhi, Y. Bando, T. Terao, C. Tang, H. Kuwahara, D. Golberg, Towards thermoconductive, electrically insulating polymeric composites with boron nitride nanotubes as fillers, *Adv. Funct. Mater.* 19 (2009) 1857–1862, <https://doi.org/10.1002/adfm.200801435>.

[2] J.K. Nelson, Y. Hu, J. Thiticharwнопong, Electrical Properties of TiO₂ Nanocomposites, *J.*, in: 2003 Annu. Rep. Conf. Electr. Insul. Dielectr. Phenom. (2003) 10–13, <https://doi.org/10.1109/CEIDP.2003.1254955>.

[3] M.T. Rahman, M.A. Hoque, G.T. Rahman, M.A. Gafur, R.A. Khan, M.K. Hossain, Evaluation of thermal, mechanical, electrical and optical properties of metal-oxide dispersed HDPE nanocomposites, *Mater. Res. Express* 6 (2019) 85092, <https://doi.org/10.1088/2053-1591/ab22d8>.

[4] K. Barber, G. Alexander, Insulation of electrical cables over the past 50 years, *IEEE Electr. Insul. Mag.* 29 (2013) 27–32, <https://doi.org/10.1109/MEI.2013.6507411>.

[5] I. Peša, P. Nožířher, C. Stancu, F. Wiesbrock, S. Schlägl, Polyethylene nanocomposites for power cable insulations, *Polymers* 11 (2018) 24, <https://doi.org/10.3390/polym11010024>.

[6] G.C. Montanari, P. Seri, L.A. Dissado, Aging mechanisms of polymeric materials under DC electrical stress: a new approach and similarities to mechanical aging, *IEEE Trans. Dielectr. Electr. Insul.* 26 (2019) 634–641, <https://doi.org/10.1109/TDEI.2018.007829>.

[7] J. Li, J. Yin, Y. Feng, Y. Liu, H. Zhao, Y. Li, C. Zhu, B. Su, D. Yue, X. Liu, Role of interface between BNNS and LDPE in excellent electrical, thermal and mechanical properties of LDPE/BNNS composites, *J. Mater. Sci. Mater. Electron.* 30 (2018) 1531–1540, <https://doi.org/10.1007/s10854-018-0424-z>.

[8] L. Boldrin, F. Scarpa, R. Chowdhury, S. Adhikari, Effective mechanical properties of hexagonal boron nitride nanosheets, *Nanotechnology* 22 (2011), <https://doi.org/10.1088/0957-4484/22/50/505702>.

[9] R. Jan, P. May, A.P. Bell, A. Habib, U. Khan, J.N. Coleman, Enhancing the mechanical properties of BN nanosheet-polymer composites by uniaxial drawing, *Nanoscale* 6 (2014) 4889–4895, <https://doi.org/10.1039/c3nr06711d>.

[10] S. Xue, Y. Wu, M. Guo, D. Liu, T. Zhang, W. Lei, Fabrication of poly(acrylic acid)/boron nitride composite hydrogels with excellent mechanical properties and rapid self-healing through hierarchically physical interactions, *Nanoscale Res. Lett.* 13 (2018), <https://doi.org/10.1186/s11671-018-2800-2>.

[11] X. Bin Wang, Q. Weng, X. Wang, X. Li, J. Zhang, F. Liu, X.F. Jiang, H. Guo, N. Xu, D. Golberg, Y. Bando, Biomass-directed synthesis of 20 g high-quality boron nitride nanosheets for thermoconductive polymeric composites, *ACS Nano* 8 (2014) 9081–9088, <https://doi.org/10.1021/nn502486x>.

[12] A.K. Naskar, J.K. Keum, R.G. Boeman, Polymer matrix nanocomposites for automotive structural components, *Nat. Nanotechnol.* 11 (2016) 1026–1030, <https://doi.org/10.1038/nnano.2016.262>.

[13] Q. Weng, X. Wang, X. Wang, Y. Bando, D. Golberg, Functionalized hexagonal boron nitride nanomaterials: emerging properties and applications, *Chem. Soc. Rev.* 45 (2016) 3989–4012, <https://doi.org/10.1039/c5cs00869g>.

[14] J. Yu, X. Huang, C. Wu, X. Wu, G. Wang, P. Jiang, Interfacial modification of boron nitride platelets for epoxy composites with improved thermal properties, *Polymer* 53 (2012) 471–480, <https://doi.org/10.1016/j.polymer.2011.12.040>.

[15] T. Sainsbury, A. Satti, P. May, Z. Wang, I. McGovern, Y.K. Gun'ko, J. Coleman, Oxygen radical functionalization of boron nitride nanosheets, *J. Am. Chem. Soc.* 134 (2012) 18758–18771, <https://doi.org/10.1021/ja3080665>.

[16] J. Shi, H. Xiong, Y. Yang, H. Shao, Nano-sized oxide filled composite PEO/PMMA/P(VDF-HFP) gel polymer electrolyte for rechargeable lithium and sodium batteries, *Solid State Ionics* 326 (2018) 136–144, <https://doi.org/10.1016/j.ssi.2018.09.019>.

[17] X. Wang, C. Zhi, Q. Weng, Y. Bando, D. Golberg, Boron nitride nanosheets: novel syntheses and applications in polymeric composites, *J. Phys. Conf. Ser.* 471 (2013), <https://doi.org/10.1088/1742-6596/471/1/012003>.

[18] X. Huang, C. Zhi, P. Jiang, D. Golberg, Y. Bando, T. Tanaka, Polyhedral oligosilsesquioxane-modified boron nitride nanotube based epoxy nanocomposites: an ideal dielectric material with high thermal conductivity, *Adv. Funct. Mater.* 23 (2013) 1824–1831, <https://doi.org/10.1002/adfm.201201824>.

[19] T.G.K. Chaffin, C. Taylor, 14-Bonding strategies and adhesives for joining medical device components, in: *Join. Assem. Med. Mater. Devices, Biomaterials*, 2013, pp. 370–404, <https://doi.org/10.1533/9780857096425.3.370>.

[20] X. Zhang, H. Wu, S. Guo, Effect of interfacial interaction on morphology and properties of polyethylene/boron nitride thermally conductive composites, *Polym. Plast. Technol. Eng.* 54 (2015) 1097–1105, <https://doi.org/10.1080/03602559.2014.974280>.

[21] J. Hou, G. Li, N. Yang, L. Qin, M.E. Grami, Q. Zhang, N. Wang, X. Qu, Preparation and characterization of surface modified boron nitride epoxy composites with enhanced thermal conductivity, *RSC Adv.* 4 (2014) 44282–44290, <https://doi.org/10.1039/c4ra07394k>.

[22] M. Cheng, A. Ramasubramanian, M.G. Rasul, Y. Jiang, Y. Yuan, T. Foroozan, R. Deivanayagam, M. Tamadoni Saray, R. Rojaee, B. Song, V.R. Yurkiv, Y. Pan, F. Mashayek, R. Shahbazian-Yassar, Direct ink writing of polymer composite electrolytes with enhanced thermal conductivities, *Adv. Funct. Mater.* (2020) 2006683, <https://doi.org/10.1002/adfm.202006683>.

[23] J.P. Hong, J.W. Shin, S.M. Hong, C.M. Koo, B.K. Baek, S. Yu, Y. Seo, W.N. Kim, J.-W. Lee, Polyethylene/boron-containing composites for radiation shielding, *Thermochim. Acta* 585 (2014) 5–9, <https://doi.org/10.1016/j.tca.2014.03.039>.

[24] S. Kango, S. Kalia, A. Celli, J. Njuguna, Y. Habibi, R. Kumar, Surface modification of inorganic nanoparticles for development of organic-inorganic nanocomposites - a review, *Prog. Polym. Sci.* 38 (2013) 1232–1261, <https://doi.org/10.1016/j.progpolymsci.2013.02.003>.

[25] A.S. Luyt, J.A. Molefi, H. Krump, Thermal, mechanical and electrical properties of copper powder filled low-density and linear low-density polyethylene composites, *Polym. Degrad. Stabil.* 91 (2006) 1629–1636, <https://doi.org/10.1016/j.polymdegradstab.2005.09.014>.

[26] P. Liu, Z. Jin, G. Katsukis, L.W. Drahushuk, S. Shimizu, C.-J. Shih, E.D. Wetzel, J. K. Taggart-Scarff, B. Qing, K.J. Van Vliet, R. Li, B.L. Wardle, M.S. Strano, Layered and scrolled nanocomposites with aligned semi-infinite graphene inclusions at the platelet limit, *Science* 353 (2016) 364–367, <https://doi.org/10.1126/science.aaf4362>, 80.

[27] L. Landel, R. Nielsen, *Mechanical Properties of Polymers and Composites*, CRC Press, Boca Raton, 1993, <https://doi.org/10.1201/b16929>.

[28] L. Shanmugam, M.E. Kazemi, Z. Rao, D. Lu, X. Wang, B. Wang, L. Yang, J. Yang, Enhanced Mode I fracture toughness of UHMWPE fabric/thermoplastic laminates with combined surface treatments of polydopamine and functionalized carbon nanotubes, *Compos. B Eng.* 178 (2019) 107450, <https://doi.org/10.1016/j.compositesb.2019.107450>.

[29] G. Zhang, T. Wu, W. Lin, Y. Tan, R. Chen, Z. Huang, X. Yin, J. Qu, Preparation of polymer/clay nanocomposites via melt intercalation under continuous elongation flow, *Compos. Sci. Technol.* 145 (2017) 157–164, <https://doi.org/10.1016/j.compscitech.2017.04.005>.

[30] M.A. Pérez, B.L. Rivas, K.A. Garrido-Miranda, V.H. Campos-Requena, M. Martínez, J. Castaño, Á. Maldonado, Low Density Polyethylene (LDPE) nanocomposites with passive and active barrier properties, *J. Chil. Chem. Soc.* 59 (2014) 2442–2446, <https://doi.org/10.4067/S0717-97072014000200009>.

[31] B.G. Choi, J. Hong, Y.C. Park, D.H. Jung, W.H. Hong, P.T. Hammond, H. Park, Innovative polymer nanocomposite electrolytes: Nanoscale manipulation of ion channels by functionalized graphenes, *ACS Nano* 5 (2011) 5167–5174, <https://doi.org/10.1021/nm2013113>.

[32] M. Abdelmouleh, S. Boufi, M.N. Belgacem, A. Dufresne, Short natural-fibre reinforced polyethylene and natural rubber composites: effect of silane coupling agents and fibres loading, *Compos. Sci. Technol.* 67 (2007) 1627–1639, <https://doi.org/10.1016/j.compscitech.2006.07.003>.

[33] E.Y. Choi, S.C. Roh, C.K. Kim, Noncovalent functionalization of multi-walled carbon nanotubes with pyrene-linked nylon66 for high performance nylon66/multi-walled carbon nanotube composites, *Carbon N. Y.* 72 (2014) 160–168, <https://doi.org/10.1016/j.carbon.2014.01.068>.

[34] Y. Zhao, E.V. Barrera, Asymmetric diamino functionalization of nanotubes assisted by BOC protection and their epoxy nanocomposites, *Adv. Funct. Mater.* 20 (2010) 3039–3044, <https://doi.org/10.1002/adfm.201000942>.

[35] J.W. Sikora, I. Gajdoš, A. Puszka, Polyethylene-matrix composites with halloysite nanotubes with enhanced physical/thermal properties, *Polymers* 11 (2019) 787, <https://doi.org/10.3390/polym11050787>.

[36] M. Terrenos, O. Martín, M. González, J. Pozuelo, B. Serrano, J.C. Cabanelas, S. M. Vega-Díaz, J. Baselga, Interphases in graphene polymer-based nanocomposites: achievements and challenges, *Adv. Mater.* 23 (2011) 5302–5310, <https://doi.org/10.1002/adma.201102036>.

[37] T.L. Chantawansri, I.C. Yeh, A.J. Hsieh, Investigating the glass transition temperature at the atom-level in select model polyamides: a molecular dynamics study, *Polymer* 81 (2015) 50–61, <https://doi.org/10.1016/j.polymer.2015.09.069>.

[38] F. Bonaccorso, L. Colombo, G. Yu, M. Stoller, V. Tozzini, A.C. Ferrari, R.S. Ruoff, V. Pellegrini, Graphene, related two-dimensional crystals, and hybrid systems for energy conversion and storage, *Science* 347 (2015) 1246501–1246509, <https://doi.org/10.1126/science.1246501>, 80.

[39] N. Tajaddod, K. Song, E.C. Green, Y. Zhang, M.L. Minus, Exfoliation of boron nitride platelets by enhanced interfacial interaction with polyethylene, *Macromol. Mater. Eng.* 301 (2016) 315–327, <https://doi.org/10.1002/mame.201500284>.

[40] M. Azeem, R. Jan, S. Farrukh, A. Hussain, Improving gas barrier properties with boron nitride nanosheets in polymer-composites, *Results Phys* 12 (2019) 1535–1541, <https://doi.org/10.1016/j.rinp.2019.01.057>.

[41] J.W. Gilman, Flammability and thermal stability studies of polymer layered-silicate (clay) nanocomposites, *Appl. Clay Sci.* 15 (1999) 31–49, <https://doi.org/10.1016/j.molstruc.2004.10.036>.

[42] B.N. Jang, C.A. Wilkie, The thermal degradation of polystyrene nanocomposite, *Polymer* 46 (2005) 2933–2942, <https://doi.org/10.1016/j.polymer.2005.01.098>.

[43] A.T. Seyhan, Y. Göncü, O. Durukan, A. Akay, N. Ay, Silanization of boron nitride nanosheets (BNNSs) through microfluidization and their use for producing thermally conductive and electrically insulating polymer nanocomposites, *J. Solid State Chem.* 249 (2017) 98–107, <https://doi.org/10.1016/j.jssc.2017.02.020>.

[44] W. Xie, Z. Gao, W.P. Pan, D. Hunter, A. Singh, R. Vaia, Thermal degradation chemistry of alkyl quaternary ammonium Montmorillonite, *Chem. Mater.* 13 (2001) 2979–2990, <https://doi.org/10.1021/cm010305s>.

[45] W. Xiea, Z. Gaoa, K. Liua, W.-P. Pana, R. Vaiab, D. Hunterc, A. Singhd, TG characterization of organically modified montmorillonite, *J. Therm. Anal. Calorim.* 75 (2004) 671–676, <https://doi.org/10.1023/B:JTAN.0000027161.10803.60>.

[46] R. Rojaee, S. Cavallo, S. Mogurampelly, B.K. Wheatle, V. Yurkiv, R. Deivanayagam, T. Foroozan, M.G. Rasul, S. Sharifi-Asl, A.H. Phakatkar, M. Cheng, S.B. Son, Y. Pan, F. Mashayek, V. Ganesan, R. Shahbazian-Yassar, Highly-cyclable room-temperature phosphorene polymer electrolyte composites for Li metal batteries, *Adv. Funct. Mater.* 30 (2020) 1910749, <https://doi.org/10.1002/adfm.201910749>.

[47] S. Narayanan, E. Firilar, M.G. Rasul, T. Foroozan, N. Farajpour, L. Covnot, R. Shahbazian-Yassar, T. Shokuhfar, On the structure and chemistry of iron oxide cores in human heart and human spleen ferritins using graphene liquid cell electron microscopy, *Nanoscale* 11 (2019) 16868–16878, <https://doi.org/10.1039/c9nr01541h>.

[48] R. Rizvi, E.P. Nguyen, M.D. Kowal, W.H. Mak, S. Rasel, M.A. Islam, A. Abdelaal, A. S. Joshi, S. Zekriardehani, M.R. Coleman, R.B. Kaner, High-throughput continuous production of shear-exfoliated 2D layered materials using compressible flows, *Adv. Mater.* 30 (2018) 1–11, <https://doi.org/10.1002/adma.201800200>.

[49] K.M.Z. Kallol, M. Motalab, M.S. Parvej, P.R. Konari, H. Barghouthi, M. Khandaker, Differences of curing effects between a human and veterinary bone cement, *Materials* 12 (2019) 1–11, <https://doi.org/10.3390/ma12030470>.

[50] M.T. Rahman, M. Asadul Hoque, G.T. Rahman, M.A. Gafur, R.A. Khan, M. K. Hossain, Study on the mechanical, electrical and optical properties of metal-oxide nanoparticles dispersed unsaturated polyester resin nanocomposites, *Results Phys.* 13 (2019) 102264, <https://doi.org/10.1016/j.rinp.2019.102264>.

[51] Q.N. Sultana, M.M. Hasan, S. Iqbal, I. Shabib, A. Mitra, M. Khan, Investigation of mechanical properties and morphology of multi-walled carbon nanotubes reinforced cellulose acetate fibers, *Fibers* 5 (2017), <https://doi.org/10.3390/fib5040042>.